Energy 70 (2014) 223–230

Contents lists available at ScienceDirect

Energy

journal homepage: www.elsevier.com/locate/energy

Bimetallic Ag–Ni/C particles as cathode catalyst in AFCs (alkaline fuel cells)

Xingjuan Song [a,b], Dongming Zhang [a,*]

[a] State Key Laboratory of Advanced Technology for Materials Synthesis and Processing, Wuhan University of Technology, Wuhan 430070, China
[b] Wuhan University of Technology, Huaxia College, Wuhan 430070, China

ARTICLE INFO

Article history:
Received 6 August 2013
Received in revised form
15 March 2014
Accepted 27 March 2014
Available online 5 May 2014

Keywords:
Cathode catalyst
Ag–Ni alloys
Heat treatment
Catalyst performance
Microstructures

ABSTRACT

AFCs (alkaline fuel cells) is one of the promising fuel cells, due to their low working temperature and less corrosive environment. However, decreasing the catalyst cost and improving its performance are still the challenges in its application. Transition metal as the catalyst for AFCs not only can reduce its cost, but also has great electro-catalytic efficiency. In this paper, Carbon supported Ag–Ni bimetallic catalysts with differential Ag/Ni atomic ratios were prepared by chemically reducing silver and nickel salts. Ag_3Ni/C shows the relatively higher ORR (oxygen reduction reaction) activity among the differential Ag/Ni bimetallic particles. In order to improve the activity and stability, the catalysts were heat-treated at the temperature of 500 °C. The results indicate that the limiting current density has been improved greatly for Ag_3Ni/C-500 °C, which is as high as 2.5× that of Ag/C. The microstructure investigation show that the non-equilibrium state of Ag–Ni alloy by heat treatment is confirmed by HRTEM (high-resolution transmission electron microscopy) images, and Ag(111) surfaces are decreased in XRD pattern, which results in the ORR activity improved and overpotential decreased. Heat treatment also has contributed to Ag–Ni/C electrochemistry stability in some degree.

1. Introduction

Renewable energies [1–4], such as wind energy, fuel cell, or biofuels, have aroused much attention in recent years because of the environmental and sustainable energy consideration. Among all kinds of fuel cells [5–7], AFCs (alkaline fuel cells) and PEMFCs (polymer exchange membrane fuel cells) are the two kinds of most promising fuel cells, due to their low working temperature and high efficiency. But AFCs have advantages over traditional PEMFCs due to alkaline media provides a less corrosive environment to the catalysts and electrode [8,9]. However, there are still significant challenges for AFCs in cathode ORR (oxygen reduction reaction), including low reaction rates, high over-potentials and low stabilities. Currently, Pt [10] and its alloys, such as Pt–Pd [11], show the best desirable performance, but its high price restricts the commercialization of AFCs. As a result, searching metal catalyst with high performance and low price has become a trend [12]. Amounts of research have shown that Ag is a good candidate to replace Pt for ORRs in alkaline solutions due to its high activity and relatively low cost [13,14]. What's more, Ag and its alloy show higher tolerance toward methanol poisoning than Pt [15,16].

Guo [17] has reported that Ag/C as the cathode catalyst in alkaline solutions promote four-electron pathway for oxygen reduction, and increasing Ag loadings on carbon support facilitate the onset potential shift positively. Although, Ag has high catalytic activity for ORR, its performance and stability still lower than Pt. The main reason is that the bind between silver and oxygen is considerably weaker than that of Pt, because d-orbital for Ag is fully occupied with electrons. So, if the d-band center position of Pt is close to the optimum [18], then pure Ag is less active for O_2 reduction because the weaker Ag–O_2 interaction makes the breaking of O–O bond more difficulty. According to current understanding, the hybridization of 5d band with empty states above the Fermi level can reduce the d-electron number. In this way, Ag alloyed with a metal of low d-orbital occupancy (such as Ni, Co, Cr, V), have the coupling effect of transferring electron from Ag so to enhance the breaking of O–O band. Lima [19] has studied Ag–Co/C as cathode catalyst for ORR in AFCs and found that Co existed in the form of Co_3O_4, which contributed to the 4-electron pathway compared to Ag/C. Sekol [20] has discovered that Ag@Pd/MWNTs were shown to be tolerant for ORR in the presence of methanol and

* Corresponding author. Tel.: +86 27 87651839; fax: +86 27 87879468.
E-mail addresses: zhangdongming71@hotmail.com, zhangdongming71@whut.edu.cn (D. Zhang).

http://dx.doi.org/10.1016/j.energy.2014.03.116
0360-5442/

ethanol in the electrolyte. R.X. Feng [21] has reported Ag–Ni catalyst for borohydride fuel cells exhibited a higher discharge voltage and capacity. But little research about Ag–Ni used in the alkaline solution has been reported until now.

This paper explores the use of Ag–Ni/C as the cathode catalyst for ORR in the alkaline electrolyte and detects the appropriate ratio between Ag–Ni. Moreover, the effect of heat treatment on Ag–Ni/C structure and catalytic activity will be discussed.

2. Experimental

2.1. Materials preparation and characterization

The catalyst support was carbon blacks Vulcan XC-72 (Cabot Corp, BET: 237 m^2/g, denoted as C). Prior to Ag–Ni deposition, firstly, Vulcan XC-72 carbon black were pre-treated with the mixed acid of nitric acid and sulfuric acid (HNO_3–H_2SO_4, concentration as13.3 M and 7.5 M) at 70 °C. The aim of this process is not only to purify XC-72 carbon blacks but also to add some surface functional groups, including carboxyl, hydroxyl and carbonyl groups.

Ag and Ag–Ni as catalyst were dispersed on carbon blacks (Ag/C or Ag–Ni/C) with percentage of 30 wt. % metal/C. The bimetallic particles were home-made with differential nominal atomic ratios, ranging from pure Ag to Ag:Ni with 3:1 and 1:3, all of which were prepared by simultaneous reduction of the precursor metal salts $AgNO_3$ and $Ni(NO_3)_2{\cdot}6H_2O$. The reduction process was carried out at 70 °C by drop with addition of an excess $NaBH_4$ (sodium borohydride) solution into carbon blacks slurry, which was prepared by suspending the acid-treated carbon powder, $AgNO_3$, $Ni(NO_3)_2{\cdot}6H_2O$ and PVP in alcohol. Then the mixture is blended in deionized water for 30 min. The resulting precipitates were filtered and dried at 60 °C. After that, the Ag–Ni/C products was heat treated under flowing Ar with a temperature ramping rate of 5 °C min^{-1}, at 500 °C for 2 h.

The catalysts powder were detected by a XRD (X-ray diffractometer) (XRD, Rigaku Ultima III) with a Cu Kα radiation ($\lambda = 0.154060$ nm) at a scanning rate of 6° min^{-1} in the 2θ range from 10°to 90°. TEM (transmission electron microscopy) micrographs were taken using a Hitachi H-800 transmission electron microscope, with an accelerating voltage of 200 kV. HRTEM (high-resolution transmission electron microscopy) was performed using JEM 2010 field emission microscopes with maximum accelerating voltages of 200 kV. EDX (energy-dispersive X-ray spectrometry) was employed with spectroscope attached to HRTEM, which was used for compositional analyses.

2.2. Preparation of working electrode and electrochemical measurements

2.9 mg of metal/C catalysts and 50 μL of a diluted Nafion solution (5%) were dispersed in 1 ml of ultra pure water with aid of ultrasonic agitation for 10 min to give a 2.84 mg ml^{-1} black suspension. The glassy carbon electrode (3 mm diameter, 0.071 cm^2) was carefully polished with emery paper and Al_2O_3 slurry and then washed ultrasonically in triply distilled water and alcohol, respectively. The film-modified electrode with metal/C catalysts was prepared by dropping the dispersed suspension (2.5 μl, 2.84 mg ml^{-1}) on the glassy carbon electrode and then evaporating the solvent naturally. Eventually the working electrode was prepared with 0.1 mg cm^{-2} catalysts.

The catalytic activity and stability were measured with a three-electrode system using an electrochemical workstation (CS350, Wuhan, China), at room temperature (25 ± 1 °C). A Pt wire was served as counter electrode and Hg/Hg_2Cl_2 (KCl saturated) was used as reference electrode. CV (cyclic voltammetry) was recorded in a 0.1 M NaOH solution with the scan rate of 50 mV s^{-1}. High purity nitrogen gas was passed for 30 min to eliminate oxygen. After preparation, the electrodes were immersed in oxygen free solutions and cycled several times between −0.6 V and 0.6 V until steady-state was reached to clean the catalyst surface. To evaluate the ORR kinetic parameters, steady state polarization measurements for the oxygen reduction were carried out in a rotating disk electrode in saturated oxygen conditions by stair step polarization technique, and the scan rate was 10 mV s^{-1}.

3. Results and discussion

3.1. Ag–Ni/C with differential Ag–Ni ratios

Fig. 1 shows the XRD patterns of the as-prepared Ag–Ni/C bimetallic materials obtained from precursors of differential compositions, for a sake of comparison, the Ag/C and Vulcan XC-72 carbon are also shown in Fig. 1. These patterns clearly show that the three diffraction peaks for 2θ values of XC-72 are 25°, 34° and 60° respectively, and $2\theta = 25°$corresponds to the (002) plane of carbon support. The Fig. 1 also shows that all the Ag/C and Ag–Ni/C patterns have four main characteristic peaks of fcc (face-centered-cubic) crystalline Ag, namely, the planes (111), (200), (220) and (311), indicating that all as-prepared catalysts mainly posses the single fcc structure. Crystal Ni has not been detected in Fig. 1.

Fig. 2 displays the TEM images of Ag/C and Ag–Ni/C systems as-prepared, the uniform distribution of catalyst particles with predominant and regular spherical shape are observed in all samples. The particle size distribution of Ag–Ni compounds is about 20–30 nm, which is much smaller than Ag/C of 40–50 nm. This means that Ag composited with Ni is contributed to the decrease of the particle size. The SAED pattern of Ag_3Ni/C as shown in Fig. 2 (d) shows the characteristic of polycrystalline fcc structure, which is agreement with XRD results. The Ni element is found in Ag–Ni composites as detected by EDS, as shown in Fig. 2(b) and (c), with Ni content of 19.9at% in Ag_3Ni/C and 36.7at% in $AgNi_3/C$ respectively. Then, what is the possible state for Ni in the Ag–Ni particles? Two possible states are confirmed to the XRD results: (1) amorphous Ni particles alone, as observed in Fig. 6(b); (2) Ag–Ni clusters with core–shell structure.

For the Ag–Ni binary system, their phase diagram shows that these two metals are immiscible and have no tendency to form any

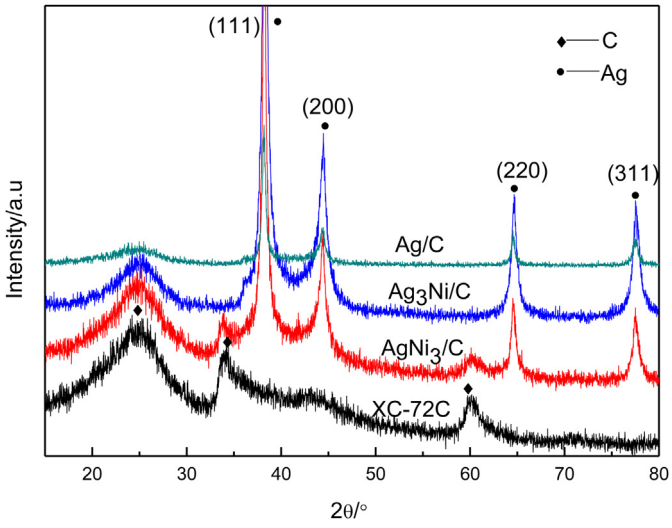

Fig. 1. X-ray diffraction patterns of Vulcan XC-72 carbon, Ag/C and Ag–Ni/C bimetallic catalysts (Ag–Ni ratios are separately 3:1 and 1:3).

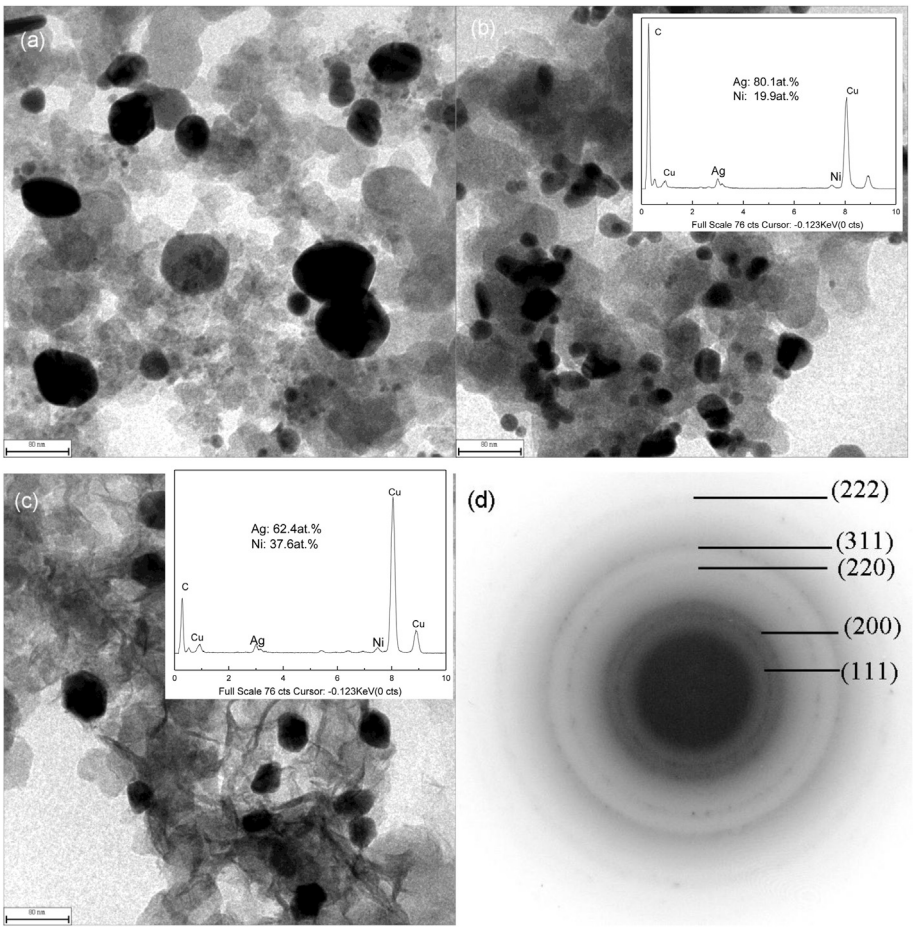

Fig. 2. TEM micrographs of the as-prepared samples: (a) Ag/C, (b) Ag_3Ni/C, (c) $AgNi_3$/C and (d) is the SAED pattern of (c).

solid solution in equilibrium state [22]. The thermodynamic assessment of the Ag–Ni binary system carried out by Liu [23] shows that the mutual solid solubility of Ag and Ni is about 1% and the solubility above the melting point is only 3%. However, many experiments and simulations have proved that Ag is easier to segregate on surface in the Ag–Ni bimetallic nano-particles and Ni core-Ag shell structure is thermodynamically favorable [24–26]. M. Harb and his coworkers have used DFT (density functional theory) to study the structure of Ag_nNi_n and found the formation of a Ni-core surrounded by silver atoms [27]. Monte Carlo simulations by Calvo showed that the Ni core-Ag shell configuration is thermodynamically stable up to 810 k [28].

So, one possible state for Ni in our experiment is with Ni core-Ag shell structure, Ni clusters are not in the state of the crystal and but buried under Ag atoms. That is why XRD can not detect Ni diffraction peaks in Ag–Ni composite particles, and HRTEM just shows Ag diffraction stripe. Similar core-cell result also has been reported in Pt–Ni system. F.GS [29] has tried to use nickel to replace parts of platinum, the results show that the nano-catalyst of Ni@Pt is formed, and its ORR activity performance is enhanced compared to Pt alone. What's more, thermal treatment in H_2 condition is favor for the Ni@Pt catalysts stabilization.

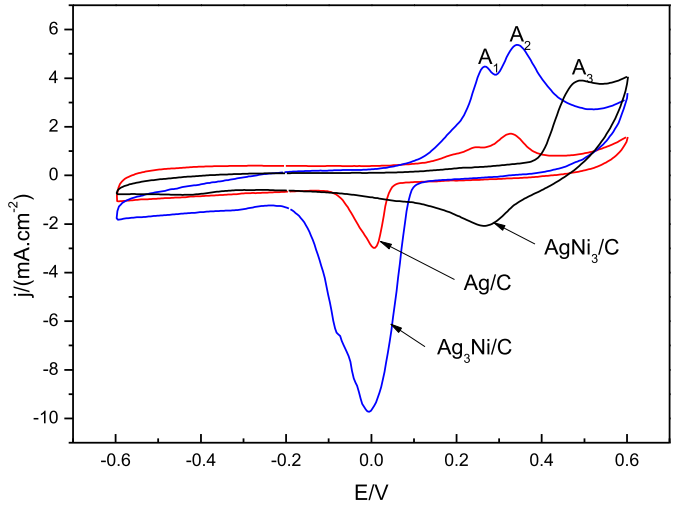

Fig. 3. CV tests for the Ag/C, Ag_3Ni/C and AgNi3/C catalysts in N_2 saturated 0.1 M NaOH electrolyte at 50 mV s^{-1}.

Fig. 3 shows the CV curves for Ag–Ni/C materials. As can be seen, Ag/C and Ag_3Ni/C have the same two anodic peaks in the range of 0.2–0.4 V, which are assigned as A_1 and A_2, standing for the formation of AgOH and Ag_2O. The cathodic peaks at around 0 V are due to the reduction of Ag_2O back to silver. The CV curves for Ag_3Ni/C catalyst does not show anodic current associated to oxidation/dissolution of Ni, demonstrating that when the ratio of Ni/Ag is low enough, core Ni can be completely covered by Ag shell. But as for $AgNi_3$/C with high ratio of Ni/Ag, core Ni can't be covered by Ag completely, so a wide peak associated with Ni oxidation at around 0.48 V [30] is observed.

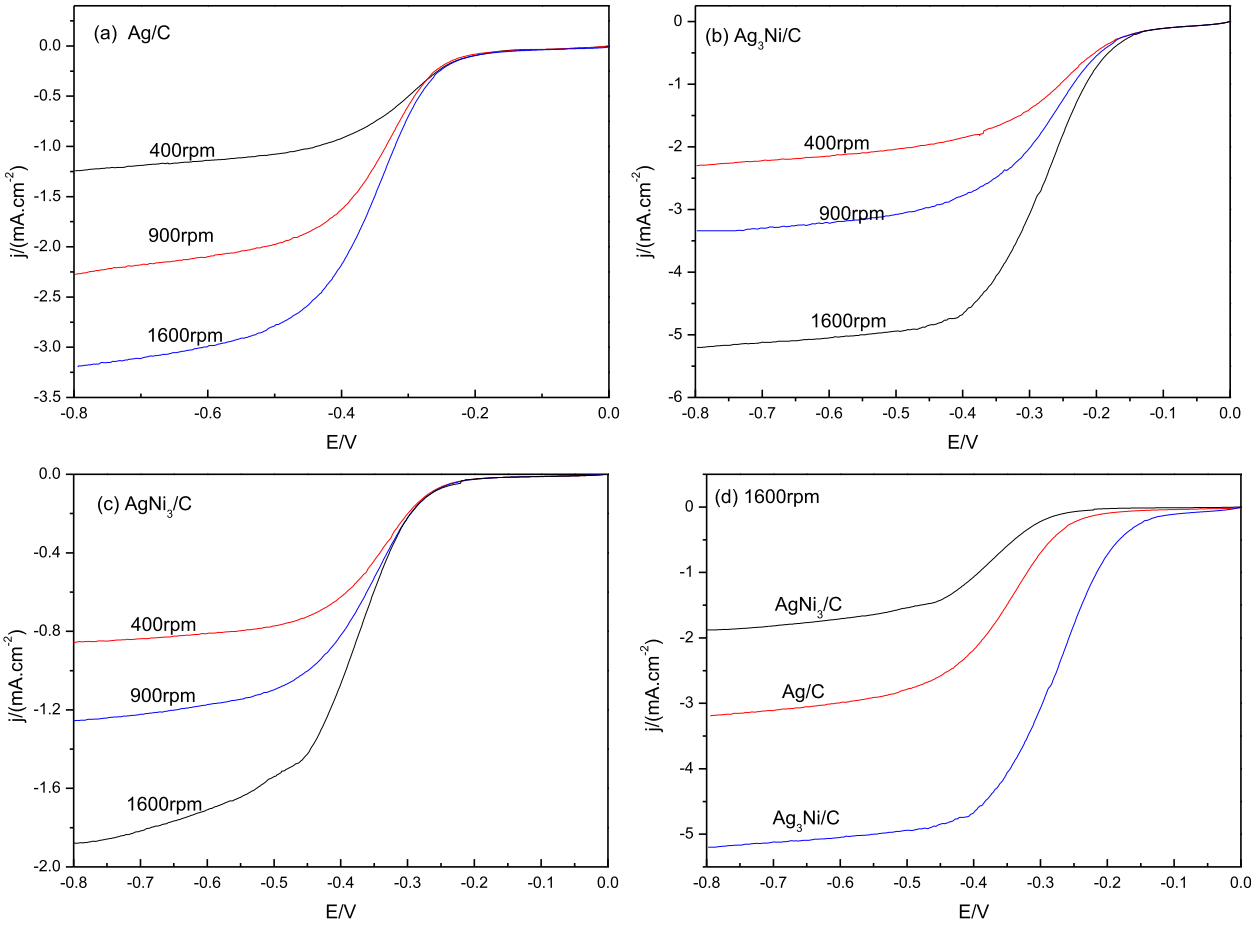

Fig. 4. Oxygen reduction polarization curves on (a) Ag/C, (b) Ag_3Ni/C and (c) $AgNi_3$/C, (d) is the their ORR curves at the same rotation rate of 1600 rpm.

The ORR polarization curves obtained on Ag/C and Ag–Ni/C catalysts at rotation rates from 400 rpm to 1600 rpm in oxygen in saturated 0.1 M NaOH solution are shown in Fig. 4. Fig. 4(a) and (b) as well as Fig. 4(c) correspond to the results of Ag/C, Ag_3Ni/C and $AgNi_3$/C respectively. It is indicated that the limiting current density increases with increasing rotation rate. As for the same rotation rate of 1600 rpm, as shown in Fig. 4(d), the limiting current density of Ag/C is higher than that of $AgNi_3$/C, but it is lower than that of Ag_3Ni/C. It is worth to notice that Ag_3Ni/C also shows the smallest overpotential compared with Ag/C and $AgNi_3$/C. Considering the performance of catalyst activity, Ag_3Ni/C is valuable to be heat treated further.

3.2. Heat treatment effect on Ag_3Ni/C

TEM micrographs of Ag_3Ni/C treated at 500 °C is shown in Fig. 5. The result indicates that the heat treatment increased the size of metal particles, and there are three types of particle size. Fig. 5(b) indicates the very small particles with 8–10 nm, which are mainly Ni particles detected by EDX. Fig. 5(c) is the HRTEM micrograph of large particles about 70–80 nm after heat treatment, and (d)–(f) are the HRTEM micrograph of moderate particles about 30–40 nm.

As it is well known that the spacing of (111) inter-plane for pure Ag and Ni is 2.4 Å and 2.0 respectively. For metals with the same crystal structure, Vegard's law predicts a simple liner relationship between alloy composition and lattice spacing. So the lattice spacing for the alloy with 25% Ag and 75% Ni is 2.1 Å, and that with 75% Ag and 25% Ni is 2.3 Å Fig. 6(e)–(f) suggest that the observed bimetallic particles have partially alloyed according to the lattice spacing [31]. The results indicate that the Ag–Ni alloy particles do exist in non-equilibrium state. Heat treatment at 500 °C stimulates the Ag–Ni alloying degree.

The XRD patterns of Ag_3Ni/C compounds annealed at 500 °C is shown in Fig. 6. Ag_3Ni/C and Ag/C as well as Ni/C-500 °C are also shown in Fig. 6(a) for comparison purpose. It is indicated that Ag_3Ni/C-500 °C retains the same fcc structure as the original Ag/C sample. But further enlarged figure (Fig. 6(b)) including Ag(111) and Ag(200) shows significant difference: (1) The diffraction peaks for Ag_3Ni/C and Ag_3Ni/C-500 °C shift to higher angles with respect to Ag/C, as listed in Table 1. As Ni atom is smaller than Ag atom, the decreased spacing of Ag(111) or Ag(200), or the diffraction angles shifted to right, suggest that some Ni atoms have been inserted into Ag crystal and form Ag–Ni solution at the Ag_3Ni/C preparation stage. As the solubility for Ag–Ni system is not enlarged by heat treatment at 500 °C, the diffraction angles stop to shift for Ag_3Ni/C-500 °C. (2) The width at half height of diffraction peak (WHHDP) is the reflection of grain sizes. WHHDPs for Ag_3Ni/C are increased, suggesting the grain sizes decreased with respect to Ag/C. Then WHHDPs are decreased by heat treatment, suggesting crystallization increasing the grain sizes, so the diffraction peaks are narrowed enough for Ag_3Ni/C-500 °C. The results are also agreement with TEM observations, as shown in Figs. 2 and 5. (3) The relative intensity of diffraction peak, I(111)/I(200) suggests the degree of crystal orientation. It is 3.7/1 for Ag/C; and 3.0/1 for Ag_3Ni/C, further more 2.5/1 for Ag_3Ni/C-500 °C by calculation, as listed in Table 1. The results indicate that the particles with Ag(111) surface are

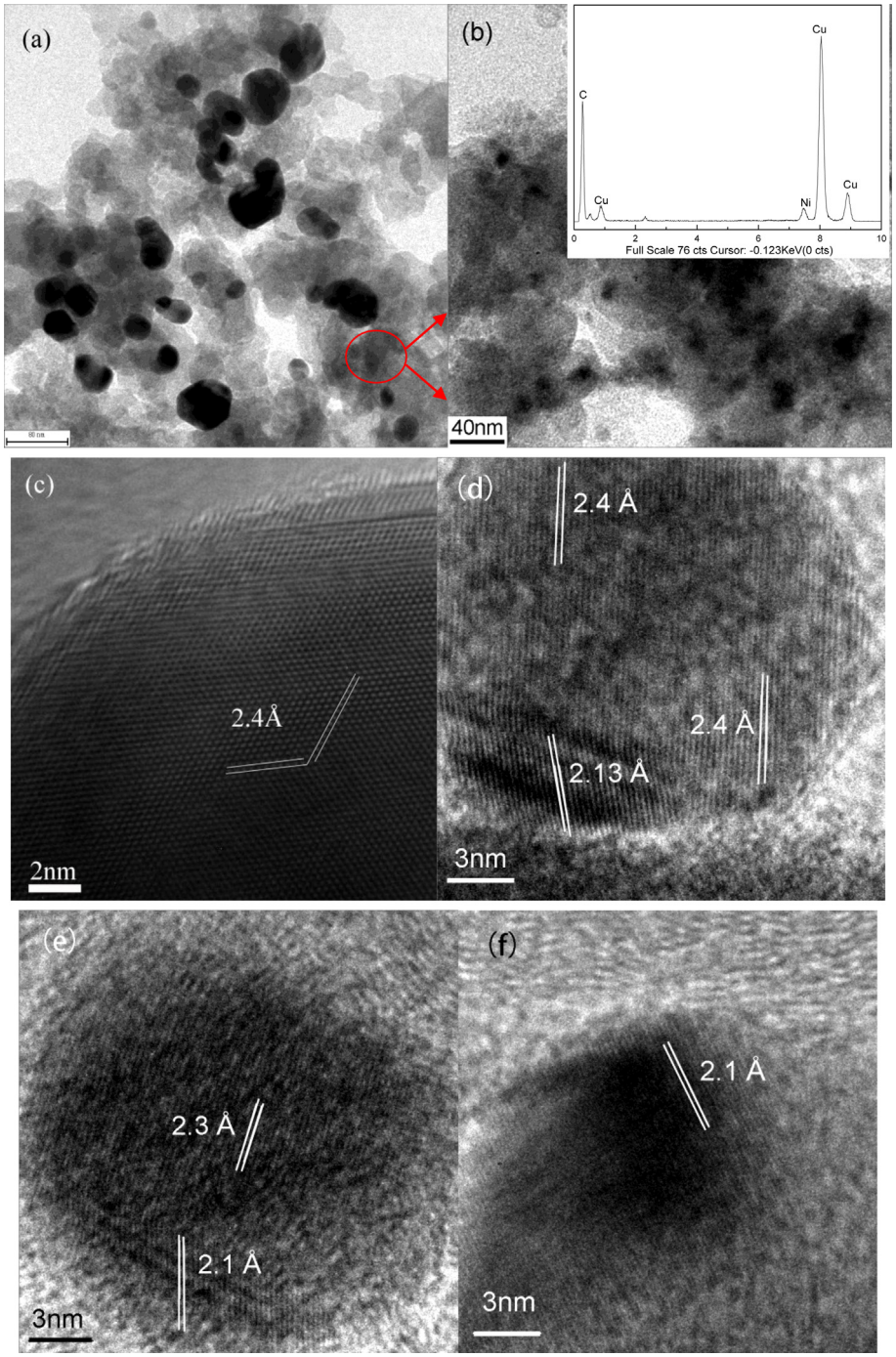

Fig. 5. (a) TEM micrographs of Ag_3Ni/C after heat treatment at 500 °C; (b) enlarged images of selected area from (a); (c) HRTEM of Ag–Ni for big particles of 90 nm; (d), (e) and (f) HRTEM of Ag–Ni particles with 30–40 nm.

decreased, but that with Ag(200), Ag(220), Ag(311) surface are increased, which may be induced by amorphous/nano Ni particles in crystallization. As amorphous/nano Ni particles are more favor to combine with nano Ag particles at the surface with closed lattice spacing, such as Ni(111)/Ag(200), or Ni(220)/Ag(311). By this way, larger Ag–Ni particles with decreased Ag(111) surface are grown in the crystallization. On the other hand, at the Ag/Ni interface, heat treatment may enhance the atom diffusion between Ag/Ni and form differential ratio of Ag–Ni alloys, as observed in Fig. 5. While from the XRD pattern in Fig. 6, the differential Ag–Ni alloying have not been detected, which suggest that every composition of alloying is no more than 5wt%.

Fig. 7 shows the CV test of Ag_3Ni/C after heat treatment at 500 °C. The anodic and cathodic peak current density of Ag_3Ni/C-500 °C are higher than that of Ag_3Ni/C. Whats more, Fig. 8(b) displays that the limiting current density of Ag_3Ni/C-500 °C is 8.2 mA cm^{-2}, which is also higher than that of Ag_3Ni/C, and is as high as 2.5 times that of Ag/C at the same rotation rate of 1600 rpm. The metal load of our prepared catalyst is 30 μg cm^{-2} (30wt% Ag_3Ni/C or 30wt%Ag/C). The comparison between Ag/C and Pt/C

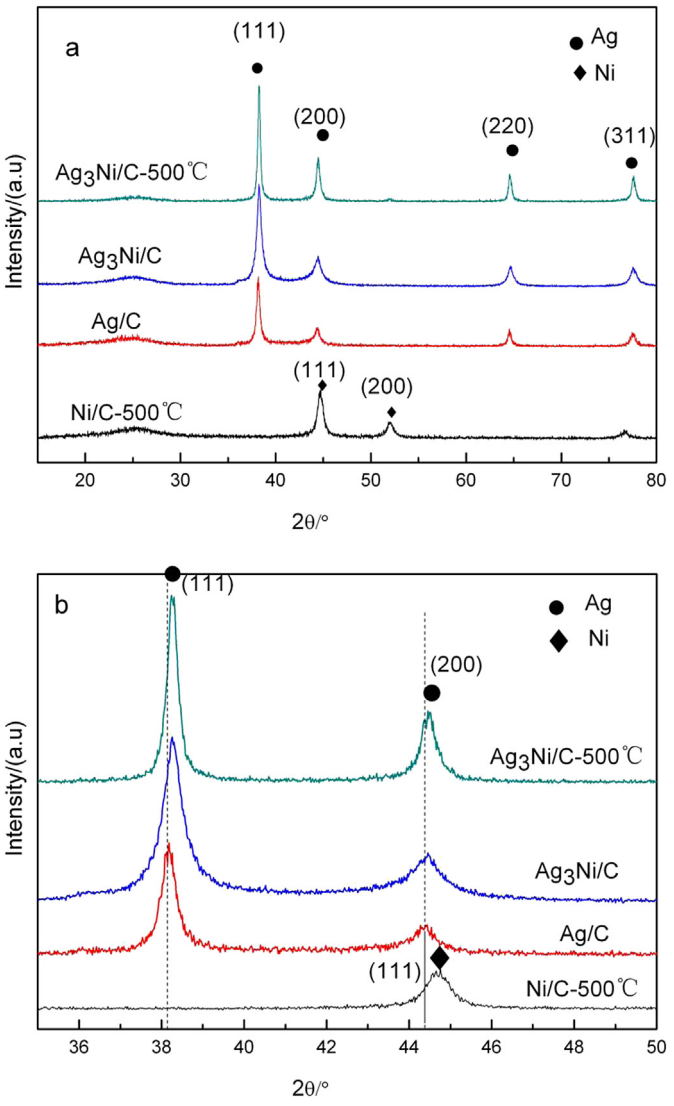

Fig. 6. XRD patterns of Ag_3Ni/C after heat treatment at 500 °C under Ar atmosphere for 2 h, and its comparison with Ag/C, Ag_3Ni/C (untreated) and Ni/C-500 °C.

reported by Demarconnay [32] and Guo [17] are similar. For example, Demarconnay [32] prepared differential Ag/C and Pt/C, and found that the limiting current density is not affected by metal loading in the range of 20wt% to 40wt%. As for 20wt%Pt/C, the limiting current density is as high as 1.2times that of 20wt%Ag/C. Xu [33] prepared 392wt%Ag/C, and found that the limiting current density is as high as 1.5 times that of 40wt%Ag/C. So the Ag_3Ni/C-500 °C prepared in this work shows higher performance than 20wt %Pt/C and 392wt%Ag/C. Considering the price ratio of Pt/Ag is about 50, the economic effect for Ag_3Ni/C-500 °C is significant.

Heat treatment also has changed the onset potential of Ag_3Ni/C-500 °C for ORR from −0.17 V to −0.15 V versus Hg/Hg_2Cl_2 (0.24 V),

Table 1
The calculated results from XRD in Fig. 5b for differential catalysts.

	Ag(111)		Ag(200)		I(111)/I(200)
	Peak/2θ	WHHDP/Δ2θ	Peak/2θ	WHHDP/Δ2θ	
Ag/C	38.188	0.434	44.420	0.766	3.7/1
Ag_3Ni/C	38.275	0.494	44.480	0.921	3.0/1
Ag_3Ni/C-500 °C	38.278	0.330	44.485	0.510	2.5/1

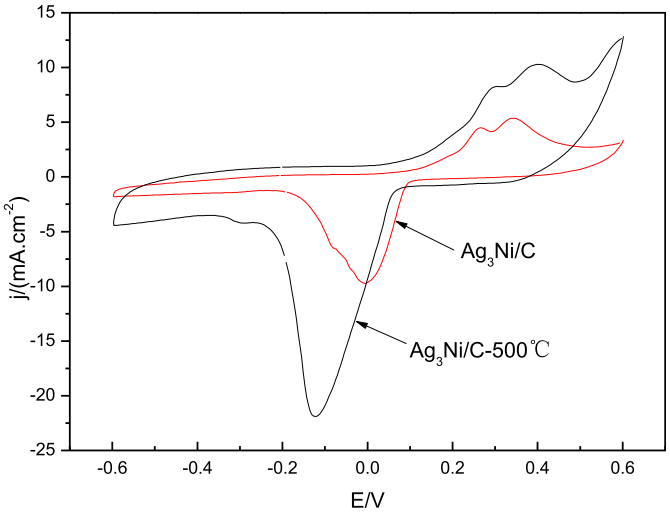

Fig. 7. CV test for the Ag_3Ni/C and $AgNi_3/C$-500 °C catalyst in N_2 saturated 0.1 M NaOH electrolyte at 50 mV s^{-1}.

because the standard potential of ORR ($O_2 + 2H_2O + 4e^- \rightarrow 4OH^-$) in alkaline solution is about 0.401 V [34], so the overpotential of Ag_3Ni/C-500 °C is 0.31 V. All these facts indicate that heat treatment is good for improving the Ag—Ni/C catalytic activity for ORR.

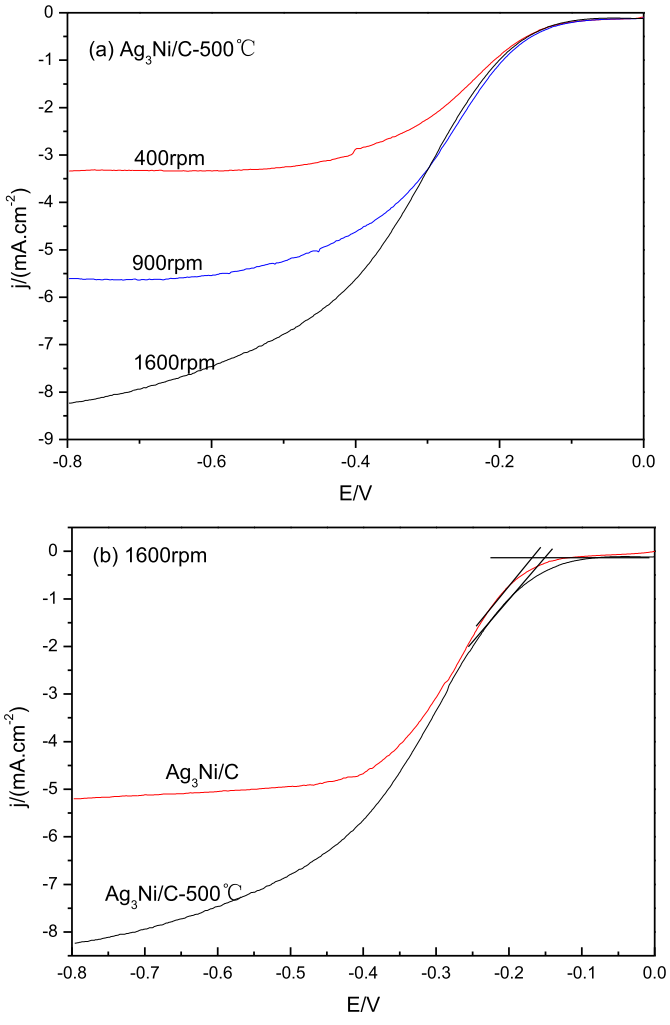

Fig. 8. Oxygen reduction polarization curves on $AgNi_3/C$ and $AgNi_3/C$-500 °C.

3.3. Accelerated durability test

As stability of catalyst in alkaline condition is very important for the application of AFC, so the durability of Ag_3Ni/C before and after heat treated has also been tested. The initial and the 100th circles by CVs of Ag_3Ni/C and Ag_3Ni/C-500 °C are shown in Fig. 9. The maximum current density and potential of Ag_3Ni/C at the same condition have altered about 59.6%, from 9.74 mA cm^{-2}/0 V for the initial to 3.94 mA cm^{-2}/0 V for the 100th circles. And Ag_3Ni/C-500 °C has decreased 50.7% from 21.9 mA cm^{-2}/-0.128 V to 10.8 mA cm^{-2}/-0.184 V. Although the stability of Ag_3Ni/C-500 °C is a little better than Ag_3Ni/C, heat treatment does not improve its stability radically.

Overall, the microstructure evolutions of the catalyst show much effect on its performance, as listed on Table 2, including Ag–Ni solution, Ag–Ni alloying, particle sizes and ratio of I(111)/I(200). (1) Ag–Ni solution and Ag–Ni alloying affect the hybridization of 5d between Ag and Ni. Ag alloyed with metal Ni of low d-orbital occupancy have the coupling effect of transferring electron from Ag to enhance the breaking of O–O band [35], and then the catalyst activity is improved by the solution and alloying effect. (2) The particles with decreased (111) surface and with increased (200), (220), (311) surface may enhance the catalyst activity. For face-centered cubic, the surface energy of (111) is the lowest.

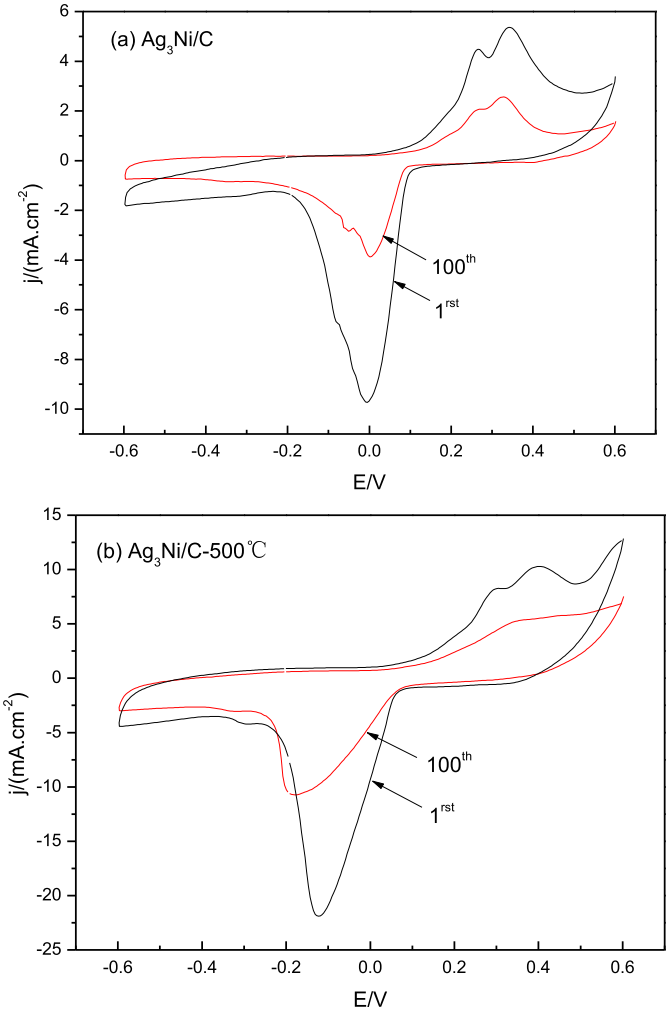

Figure.9

Fig. 9. The first and 100th circles by CV test of Ag_3Ni/C and Ag_3Ni/C-500 °C.

Table 2
The microstructure evolutions and the effects on the catalyst performance.

	Ag–Ni solution	Ag–Ni alloying	Particle sizes	Ag(111) surfaces	Limiting current density for ORR
Ag/C			large	More	I_{Ag}
Ag_3Ni/C	Yes		small	less	1.6 I_{Ag}
Ag_3Ni/C-500 °C	Yes	Yes	large	The lest	2.5 I_{Ag}

The catalyst with high-index facets shows higher catalyst activity because of the high surface energy [36]. (3) The smaller particles sizes enhance the catalyst activity, when the surface orientation is the same. The differential evolution listed on Table 2 show that, for Ag_3Ni/C, the decreased particle sizes and Ag–Ni solution are responsible for enhancing the catalyst activity. For Ag_3Ni/C-500 °C, less Ag (111) surface by crystallization and Ag–Ni alloying are responsible for enhancing the catalyst activity. Though heat treatment has increased the Ag_3Ni/C-500 °C particles sizes, but they are different from the original Ag/C particles, as those with less Ag(111) surfaces are favor to ORR.

4. Conclusion

Ag–Ni/C bimetallic catalysts of differential Ag/Ni atomic ratios can be synthesized by the solution route using $NaBH_4$ as a reducing agent. In order to improve activity and stability, the catalysts were heat-treated in the temperature of 500 °C. The measurements indicated that the addition of Ni into Ag decreased its ORR over-potential and increased its limiting current density because of the formation of Ag–Ni solution and decreased particles size. Heat treatment is good for improving the catalytic activity of Ag_3Ni/C due to the decreased Ag(111) surfaces and enhanced Ag–Ni alloying degree. The limiting current density for Ag_3Ni/C-500 °C is as high as 2.5 times that of Ag/C, while the stability of the catalyst is still not high enough.

Acknowledgments

This work is supported by National Natural Science Foundation of China (51171134 and A3 Foresight Program 50821140308) and Foundation of SKLWUT (2013-PY-5).

References

[1] Lawlor V, Griesser S, Buchinger G, Olabi AG, Cordiner S, Meissner D. Review of the micro-tubular solid oxide fuel cell: part I: stack design issues and research activities. J Power Sources 2009;193:387–99.
[2] Lawlor V. Review of the micro-tubular solid oxide fuel cell (part II: cell design issues and research activities). J Power SourceS 2013;240:421–41.
[3] Russo D, Dassisti M, Lawlor V, Olabi AG. State of the art of biofuels from pure plant oil. Renew Sustain Energy Rev 2012;16:4056–70.
[4] Carton JG, Olabi AG. Wind/hydrogen hybrid systems: opportunity for Ireland's wind resource to provide consistent sustainable energy supply. Energy; 2010: 4536–44.
[5] Esmaeilifar A, Rowshanzamir S, Eikani MH, Ghazanfari E. Synthesis methods of low-loading electrocatalysts for proton exchange membrane fuel cell systems. Energy 2010;35:3941–57.
[6] Fofana D, Natarajan SK, Hamelin J, Benard P. Low platinum, high limiting current density of the PEMFC(proton exchange membrane fuel cell) based on multilayer cathode catalyst approach. Energy 2014;64:398–403.
[7] Borghei M, Scotti G, Kanninen P, Weckman T, Anoshkin IV, Nasibulin AG, et al. Enhanced performance of a silicon microfabricated direct methanol fuel cell with PtRu catalysts supported on few-walled carbon nanotubes. Energy 2014;65:612–20.
[8] Bidaulta F, Brettb DJL, Middletonc PH, Brandon NP. Review of gas diffusion cathodes for alkaline fuel cells. J Power Sources 2009;187(1):39–48.
[9] Varcoe JR, Slade RCT. Prospects for alkaline anion-exchange membranes in low temperature fuel cells. Fuel Cells 2005;5(2):187–200.
[10] Karim NA, Kamarudin SK. Overview on non-platinum cathode catalysts for direct methanol fuel cell. Appl Energy 2013;103:212–20.

[11] Karim K, Hussien G. Palladium nanoparticle catalysts synthesis on grapheme in sodium dodecyl sulfate for oxygen reduction reaction. Energy; 2013:1–6.
[12] Huang CH, Liu SJ, Hwang WS. Chelating agent assisted heat treatment of carbon supported cobalt oxide nanoparticle for use as cathode catalyst of polymer electrolyte membrane fuel cell (PEMFC). Energy 2011;36:4410–4.
[13] Kostowskyj MA, Gilliam RJ, Kirk DW, Thorpe SJ. Silver nanowire catalysts for alkaline fuel cells. Int J Hydrogen Energy 2008;33:5773–8.
[14] Wagner N, Schulze M, Gülzow E. Long term investigations of silver cathodes for alkaline fuel cells. J Power Sources 2004;127:264–72.
[15] Demarconnay L, Coutanceau C, Léger J-M. Electroreduction of dioxygen (ORR) in alkaline medium on Ag/C and Pt/C nanostructured catalysts—effect of the presence of methanol. Electrochim Acta 2004;49(25):4513–21.
[16] Ju JF, Chen X, Shi YJ, Wu DH, Hua P. A novel TiO2 nanofiber supported PdAg catalyst for methano electr-oxidation. Energy 2013;59:478–83.
[17] Guo JS, Hsu A, Chu D, ChenImproving RR. Improving oxygen reduction reaction activities on carbon-supported Ag nanoparticles in alkaline solutions. J Phys Chem C 2010;114(10):4324–30.
[18] Zhang J, Vukmirovic MB, Xu Y, Mavrikakis M, Adzic RR. Controlling the catalytic activity of platinum-monolayer electrocatalysts for oxygen reduction with different substrates. Angew Chem 2005;44(14):2132–5.
[19] Lima FHB, Castro de JFR, Edson A. Silver-cobalt bimetallic particles for oxygen reduction in alkaline media. J Power Sources 2006;161(27):806–12.
[20] Sekol RC, Li XK, Cohen P, Doubek G, Carmo1 M, Taylor AD. Silver palladium core–shell electrocatalyst supported on MWNTs for ORR in alkaline media. Appl Catal B Environ 2013;138:285–93.
[21] Feng RX, Dong H, Cao YL, Ai XP, Yang HX. Agni-catalyzed anode for direct borohydride fuel cells. Int J Hydrogen Energy 2007;32(17):4544–9.
[22] Baker H, editor. ASM handbook. Alloy phase diagrams. Materials Park: ASM International; 1992. p. 3.
[23] Liu XJ, Gao F, Wang CP, Ishida K. Thermodynamic assessments of the Ag–Ni binary and Ag–Cu–Ni ternary systems. J Electron Mater 2008;37(2):210–7.
[24] Rapallo A, Rossi G, Ferrando R, Fortunelli A, Curley BC, Lloyd LD, Tarbuck GM, Johnston RL. Global optimization of bimetallic cluster structures. I. Size-mismatched Ag–Cu, Ag–Ni, and Au–Cu systems. J Chem Phys 2005;122(19):194308.
[25] Negreiros FR, Kuntová Z, Barcaro G, Rossi G, Ferrando R, Fortunelli A. Structures of gas-phase Ag–Pd nanoclusters: a computational study. J Chem Phys 2010;132(23):234703.
[26] Harb M, Rabilloud F, Simon D. Structure and optical properties of core-shell bimetallic Ag_nNi_n clusters: composition with pure silver and nikel clusters. J Phys Chem A 2009;131:174302.
[27] Gaudry M, Cottancin E, Pellarin M, Lerme J. Size and composition dependence in the optical properties of mixed (transition metal/noble metal) embedded clusters. Phys Rev B 2003;67(15):155409.
[28] Calvo F, Cottancin E, Broyer M. Segregation, core alloying, and shape transitions in bimetallic nanoclusters: Monte Carlo simulations. Phys Rev B 2008;77(12).
[29] GS F, HL M, SF O. Enhanced electroactivity for the oxygen reduction on Ni@pt core-shell nanocatalysts. Int J Hydrogen Energy 2012;37(19):14902–10.
[30] Aytac A, Gürbüz M, Elif SA. Electrooxidation of hydrogen peroxide and sodium borohydride on Ni deposited carbon fiber electrode for alkaline fuel cells. Int J Hydrogen Energy 2011;36:10013–21.
[31] Zhang ZY, Nenoff TM, Huang JY, Berry DT, Provencio PP. Room temperature synthesis of thermally immiscible Ag-Ni nanoalloys. J Phys Chem Lett 2009;113:1155–9.
[32] Demarconnay L, Coutanceau C, Leger JM. Electroreduction of dioxygen (ORR) in alkaline medium on Ag/C and Pt/C nanostructured catalysts-effect of the presence of methanol. Electrochim Acta 2004;49:4513–21.
[33] Xu X, Tan C, Liu H, Wang F, Li Z, Liu J, Ji J. Carbon black supported ultra-high loading silver nanoparticle catalyst and its enhanced electrocatalytic activity towards oxygen reduction reaction in alkaline medium. J Electroanal Chem 2013;696:9–14.
[34] Song C, Zhang J. Electrocatalytic oxygen reduction reaction. In: Zhang J, editor. PEM fuel cell electrocatalysts and catalyst layers. London: Sp.
[35] Wang Y, Balbuena PB. Design of oxygen reduction bimetallic catalyst: Ab initio-derived thermodynamic guidelines. J Phys Chem B 2005;109:18902–6.
[36] Tian N, Zhou Z, Sun SG. Synthesis of tetrahexahedral Platinum nanocrystals with high-index faces and high electro-oxidation activity. Science 2007;316:732–5.